Probing modified gravitational-wave propagation through tidal measurements of binary neutron star mergers

Nan Jiang⬤ and Kent Yagi⬤

Department of Physics, University of Virginia, Charlottesville, Virginia 22904, USA

Gravitational-wave sources can serve as standard sirens to probe cosmology by measuring their luminosity distance and redshift. Such standard sirens are also useful to probe theories beyond general relativity with a modified gravitational-wave propagation. Many of previous studies on the latter assume multimessenger observations so that the luminosity distance can be measured with gravitational waves while the redshift is obtained by identifying sources' host galaxies from electromagnetic counterparts. Given that gravitational-wave events of binary neutron star coalescences with associated electromagnetic counterpart detections are expected to be rather rare, it is important to examine the possibility of using standard sirens with gravitational-wave observations alone to probe gravity. In this paper, we achieve this by extracting the redshift from the tidal measurement of binary neutron stars that was originally proposed within the context of gravitational-wave cosmology (another approach is to correlate "dark sirens" with galaxy catalogs that we do not consider here). We consider not only observations with ground-based detectors (e.g., Einstein Telescope) but also multiband observations between ground-based and space-based (e.g., DECIGO) interferometers. We find that such multiband observations with the tidal information can constrain a parametric non-Einsteinian deviation in the luminosity distance (due to the modified friction in the gravitational wave evolution) more stringently than the case with electromagnetic counterparts by a factor of a few. We also map the above-projected constraints on the parametric deviation to those on specific theories and phenomenological models beyond general relativity to put the former into context.

I. INTRODUCTION

A historic detection of gravitational waves (GWs) was made September 14, 2015, by the Laser Interferometer Gravitational-wave Observatory (LIGO) in Hanford and Livingston. The GW event is known as GW150914 [1] and consists of a merger of a binary black hole (BBH). So far, nearly 50 BBH merger GW events have been found [2]. Another milestone observation was made in 2017 when LIGO and Virgo detected GW signals from a coalescing binary neutron star (BNS), known as GW170817 [3]. This event marked the dawn of multimessenger astronomy as not only GW signals but also their associated electromagnetic (EM) counterparts were detected [4]. A second BNS event, GW190425 [5], was found in the third observing run by the LIGO/Virgo Collaboration (LVC), though no electromagnetic counterpart is confirmed yet.

GW170817 serves as a standard siren to probe cosmology, in particular measuring the Hubble constant [6–8]. This constant is inferred from the independent measurement of the luminosity distance and the redshift of the source. The former is measured from the GW amplitude while the latter is obtained by identifying the host galaxy through EM counterpart observations.

Another important application of GW170817 is to test general relativity (GR). Going beyond GR is motivated by the unification of GR and the Standard Model [9–11], and it can also explain some of unsolved problems in cosmology, such as dark matter and dark energy problems [12–16]. GR has passed all the tests put to it, including solar system experiments [17] in the weak-field regime, binary pulsar observations [18,19] in the strong/nondynamical regime and GW observations [20–24] in the strong/dynamical regime. GW170817 has been used to probe the modified dispersion relation of GWs. For example, the comparison of the arrival time difference between GW and EM wave signals placed a bound on the fractional difference in the propagation speed of GWs with respect to the speed of light to be one part in 10^{-15} [4].

Standard sirens like GW170817 can also probe other aspects of the modified GW propagation, in particular the modified friction term in the GW evolution. This in turn modifies the GW amplitude from its GR counterpart, and thus the luminosity distance measured with GWs may differ from that measured through EM observations. Alternatively, one can use the luminosity distance and redshift measurement of standard sirens to probe both

cosmology and modified GW propagation. This has been demonstrated for future GW observations with advanced LIGO with its design sensitivity, Einstein Telescope (ET), and Laser Interferometer Space Antenna (LISA) [16,25–27], assuming that the luminosity distance is measured through GWs while the redshift is obtained from that of the host galaxy that is identified through EM counterparts. If there are no associated EM counterparts, one can still use such GW sources "dark sirens" to probe cosmology and gravity by taking their correlation with galaxy catalogs [28,29].

In this paper, we study an alternative approach of using standard sirens without EM counterparts to probe the modified GW propagation through tidal effects of BNSs. This idea was first proposed in [30] within the context of probing cosmology with GW observations alone. The authors in [30] realized that the tidal deformability that characterizes tidal effects in a BNS depends on the intrinsic mass, so together with the measurement of the redshifted mass, one can infer the source's redshift provided that one knows the nuclear matter equation of state *a priori*.

We here apply the above methodology to tests of modified GW propagation (or modified GW friction) to study how much improvement one gains from the case where one uses only BNSs with EM counterparts. We follow [16,25] and work in a generic modified GW parametrization (Ξ_0, n), where Ξ_0 represents the ratio between the luminosity distance measured by GW and EM signals at large z while n denotes the redshift dependence on the ratio. Such a generic parametrization has a known mapping to theoretical constants in some specific non-GR theories [16]. We carry out a Fisher analysis to derive projected bounds on Ξ_0 for various n with ET and multiband GW observations. The latter is a joint observation between ground- and space-based interferometers [31–38]. Here, we focus on multiband observations between ET and DECihertz laser Interferometer Gravitational wave Observatory (DECIGO) [39,40]. B-DECIGO, the scientific pathfinder of DECIGO, is planned to be launched in the 2030s [40], while DECIGO is expected to be launched at a later time.

We here present a brief summary of our findings. We first compute the measurability of the BNS redshift with GW observations alone, and find that multiband observations improve the accuracy by $\sim 50\%$ compared to the case with ET only. Next, we show the bound on the modified GW propagation parameter Ξ_0. Figure 1 presents such a bound against the fraction α of BNS events within the redshift range of $z = [0.1, 2]$ whose redshift is identified through EM counterparts. We choose a representative case of $n = 2.5$ and SLy equation of state (EOS). Observe that the addition of BNSs without EM counterparts improves the bound by a factor of a few in the case of ET alone, and the bound further improves further if one uses multiband observations. Although the figure is only for $n = 2.5$, we
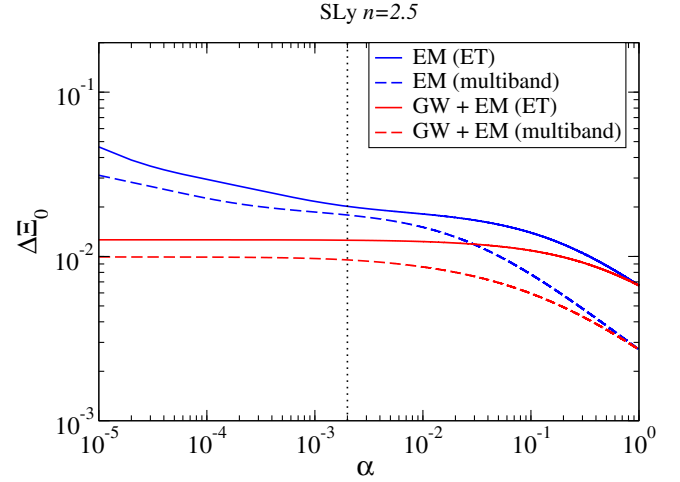

FIG. 1. Measurability of the modified GW propagation parameter Ξ_0 as a function of the fraction α of the events with redshift identification through EM counterparts. We show results for (i) using only BNS events with EM counterparts ("EM" as in Eq. (37), as done in previous literature) and (ii) combining BNS events with and without EM counterparts ("GW + EM" in Eq. (38). We consider observations with ET alone and multiband observations (with an observation time of 3 yrs for the latter). We use SLy EOS and set $n = 2.5$ in Eq. (3). The vertical dashed line at $\alpha = 2 \times 10^{-3}$ corresponds to the typical fraction of BNSs with EM counterparts [41]. Observe that the addition of BNSs without EM counterparts improves the measurability from those with EM counterpart by a factor of a few.

find that the bound on Ξ_0 is insensitive to the choice of n. Lastly, we map the bound on Ξ_0 to parameters in specific non-GR theories. In the case of a scalar-tensor theory, for example, the relevant parameter can be constrained to a level of $\sim 10^{-2}$.

The organization of the rest of the paper is as follows. In Sec. II, we briefly introduce the formalism of how the modified luminosity distance is parameterized and the mapping between this theory-agnostic parametrization and constants in specific non-GR theories like scalar-tensor theories and phenomenological models. In Sec. III, we will explain how to estimate uncertainties of the redshift measurement for a BNS event without EM counterpart from the tidal effect in the gravitational waveform. Section IV describes the Fisher analysis for parameter estimation on the redshift and non-GR parameters. We present our results on the measurability of the redshift, modified GW propagation parameter and theory-specific parameters in Sec. V. In Sec. VI, we give concluding remarks and describe avenues for possible works. We use the unit $G = c = \hbar = 1$ throughout.

II. MODIFIED LUMINOSITY DISTANCE

GW sources can be used as standard sirens to probe cosmology from the relation between the luminosity

distance d_L and the redshift z [6,42,43]. Such sources can also be used to probe gravity since the above relation not only depends on cosmological parameters but also on the underlying gravitational theory.

A. Formalism

One can, in particular, probe generic theories that modifies the Hubble friction term in the propagation equation of GWs [25][1]:

$$\tilde{h}_A'' + 2\mathcal{H}[1 + \alpha_M(\eta)]\tilde{h}_A' + k_{\text{gw}}^2 \tilde{h}_A = 0. \qquad (1)$$

Here $\tilde{h}_A$ is the metric perturbation (or GW amplitude) in the Fourier domain with $A = +, \times$ representing the plus and cross polarization modes, a prime representing the derivative with respect to the conformal time η, k_{gw} is the wave number, $\mathcal{H} \equiv a'/a$ with a denoting the scale factor, and $\alpha_M(\eta)$ is the modified friction term. The above equation reduces to the one in GR when $\alpha_M = 0$. The friction term modification affects the GW amplitude, which can be absorbed into the luminosity distance. This leads to a difference in the luminosity distance measured through GWs $d_L^{\text{gw}}(z)$ and EM waves $d_L^{\text{em}}(z)$ as follows [25,46]:

$$d_L^{\text{gw}}(z) = d_L^{\text{em}}(z) \exp\left[\int_0^z \frac{\alpha_M(z)}{1+z} dz\right]. \qquad (2)$$

A useful parametrization has been proposed in [25] as

$$\frac{d_L^{\text{gw}}(z)}{d_L^{\text{em}}(z)} = \Xi_0 + \frac{1 - \Xi_0}{(1+z)^n}. \qquad (3)$$

Here Ξ_0 corresponds to the constant ratio of the luminosity distance in the limit $z \to \infty$ while n shows the redshift dependence of the ratio. GR is recovered when $\Xi_0 \to 1$ and this is the case when $z \to 0$. Such a parametrization allows us to treat the modification in the luminosity distance measurement from GWs in a generic way, and at the same time to map the modified GW propagation parameters (Ξ_0, n) to theoretical constants in known gravitational theories beyond GR.

B. Mapping to scalar-tensor theories and phenomenological models

In this paper, we consider scalar-tensor theories and phenomenological models as specific examples [16].

---

[1]In general, the last term on the left-hand side of Eq. (1) can acquire non-GR corrections that modify the propagation speed of GWs and/or add a mass to the graviton, and an anisotropic stress source term may arise on the right-hand side (see, e.g., [44,45]).

1. Horndeski theories

Let us first review scalar-tensor theories. We consider, in particular, theories within Horndeski theories [47], which are most general scalar-tensor theories with field equations containing up to second order derivatives (see, e.g., [48] for a recent review). The action is given by [16]

$$S = \int d^4x \sqrt{-g}\left[\sum_{i=2}^{5} \mathcal{L}_i + \mathcal{L}_{\text{m}}(g_{\mu\nu}, \psi_{\text{m}})\right] \qquad (4)$$

with Lagrangian densities

$$
\begin{aligned}
\mathcal{L}_2 &= G_2(\phi, X), \\
\mathcal{L}_3 &= G_3(\phi, X)\Box\phi, \\
\mathcal{L}_4 &= G_4(\phi, X)R - 2G_{4X}(\phi, X)[(\Box\phi)^2 - (\nabla_\mu\nabla_\nu\phi)^2], \\
\mathcal{L}_5 &= G_5(\phi, X)G_{\mu\nu}\nabla^\mu\nabla^\nu\phi + \frac{1}{3}G_{5X}(\phi, X) \\
&\quad \times [(\Box\phi)^3 - 3\Box\phi(\nabla_\mu\nabla_\nu\phi)^2 + 2(\nabla_\mu\nabla_\nu\phi)^3],
\end{aligned}
$$

where ϕ is the scalar field, $X \equiv \partial_\mu\phi\partial^\mu\phi$, R and $G_{\mu\nu}$ represent the Ricci scalar and Einstein tensor in the Jordan frame metric $g_{\mu\nu}$. $G_i(\phi, X)$ are arbitrary functions of ϕ and X and $G_{iX} \equiv \partial G_i/\partial X$. The matter field ψ_{m} in the Lagrangian density for matter $\mathcal{L}_m$ is minimally coupled to gravity. Given that GW170817 placed a stringent bound on the propagation speed of GWs c_{gw} [4,49], we consider $G_{4X} = 0$ and $G_5 = \text{const.}$, which guarantees that $c_{\text{gw}} = 1$ [50–52].

The correction to the Hubble friction term is related to G_4 through the effective Planck mass M_{eff} as

$$\alpha_M = \frac{d\ln M_{\text{eff}}^2}{d\ln a}, \qquad M_{\text{eff}}^2 = 2G_4. \qquad (5)$$

The modified GW propagation parameters are given by [16]

$$\Xi_0 = \lim_{z\to\infty}\frac{M_{\text{eff}}(0)}{M_{\text{eff}}(z)}, \qquad n \approx \frac{\alpha_{M0}}{2(\Xi_0 - 1)}, \qquad (6)$$

where α_{M0} is α_M at the present time.

As an example of Horndeski theories, we consider $f(R)$ gravity where the Einstein-Hilbert action is modified with $R \to R + f(R)$ for an arbitrary function f. G_4 then becomes

$$G_4 = \frac{1 + f_R}{2}M_{\text{P}}^2, \qquad (7)$$

where M_{P} is the Planck mass that is related to the effective Planck mass as $M_{\text{P}} = \lim_{z\to\infty}M_{\text{eff}}(z)$. $f_R \equiv f'(R)$ and a prime represents a derivative with respect to R. For such a model, Ξ_0 and n are given by

TABLE I. Mapping of the modified GW propagation parameters (Ξ_0, n) to parameters in scalar-tensor theories (top) and phenomenological models for α_M or the effective Planck mass M_{eff} (bottom) [16].

Non-GR Model	$\Xi_0 - 1$	n
HS $f(R)$ [53]	$\frac{1}{2}f_{R0}$	$\frac{3(\bar{n}+1)\Omega_M}{4-3\Omega_M}$
designer $f(R)$ [54]	$-0.24\Omega_M^{0.76}B_0$	$3.1\Omega_M^{0.24}$
Brans-Dicke [55]	$\frac{1}{2}\delta\phi_0$	$\frac{3(\bar{n}+1)\Omega_M}{4-3\Omega_M}$
power law α_M [56]	$\frac{\alpha_{M0}}{2\bar{n}}$	$\bar{n}$
DE density α_M [56,57]	$-\frac{\alpha_{M0}}{6\Omega_\Lambda \ln\Omega_M}$	$-\frac{3\Omega_\Lambda}{\ln\Omega_M}$
power law M_{eff} [58]	$\frac{1}{2}\Omega_+$	$\bar{n}$

$$\Xi_0 = \sqrt{1+f_{R0}} \approx 1 + \frac{1}{2}f_{R0}, \tag{8}$$

$$n \approx \left(\frac{f_R'}{f_R}\right)_0, \tag{9}$$

where the subscript 0 corresponds to the present value. In particular, we consider a model proposed by Hu and Sawicki (HS). Ξ_0 and n for the HS $f(R)$ gravity are given in Table I where $\bar{n}$ is a positive integer and Ω_M is the matter energy density parameter.

$f(R)$ gravity is a special case of Brans-Dicke theory [55]. G_4 and G_2 in the latter theory is given by

$$G_4(\phi) \equiv \frac{M_P^2\phi}{2}, \tag{10}$$

and $G_2 = -U(\phi) + X\omega(\phi)/\phi$, where ω is the Brans-Dicke function and U is the scalar field potential. The theory reduces to $f(R)$ gravity when $\omega = 0$. The mapping of (Ξ_0, n) to Brans-Dicke theory is given in Table I, where $\delta\phi_0 \equiv \phi_0 - 1$.

2. Phenomenological models

The second model we consider is a phenomenological parametrization on α_M motivated by a time-varying effective Planck mass M_{eff}. We consider two different parametrization for α_M:

(i) power law:

$$\alpha_M = \alpha_{M0}a^{\bar{n}}; \tag{11}$$

(ii) dark energy density:

$$\alpha_M = \alpha_{M0}\frac{\Omega_\Lambda(a)}{\Omega_{\Lambda 0}}, \tag{12}$$

where Ω_Λ is the dark energy density parameter. Once again, Ξ_0 and n for these models are summarized in Table I.

In Appendix A, we review other models within Horndeski theories and phenomenological classes, and give the mapping to (Ξ_0, n) in Table I.

III. REDSHIFT INFERENCE THROUGH TIDAL EFFECTS

To probe gravity from the luminosity distance-redshift relation in Eq. (3), one needs an independent measurement of d_L and z. The former is measured from the amplitude of GWs while the latter is more challenging to measure as it typically degenerates with the mass. If a BNS event has an associated EM counterpart, one can use the redshift information of the host galaxy, which has been used for GW170817 to measure the Hubble constant [6] and also to give future forecasts on testing the modified GW propagation [25]. However, BNS events with EM counterparts are expected to be rare, with a fraction of only $\sim 10^{-3}$ or so [41].

An alternative method to measure the redshift with GW observations alone is to use the tidal effect [30]. Such an effect in BNS is characterized by tidal deformabilities or Love numbers that depend on the intrinsic (source-frame) masses of NSs. Together with the redshifted mass measurement, one can break the degeneracy between the redshift and the mass to extract the former. This method requires one to know the nuclear matter equation of state *a priori* which still has relatively large uncertainties. One may use future GW observations of nearby BNS sources ($z \lesssim 0.1$) with EM counterparts to determine the equation of state, and use those of BNSs with large z to probe the modified GW propagation [30,59].

Let us explain this tidal method in more detail by taking NRTidalv2 [60,61] as an example. The tidal contribution to the gravitational wave phase in the frequency domain is given by

$$\psi_T(x) = -\frac{13}{8\nu}\kappa_{\text{eff}}x^{5/2}P(x), \tag{13}$$

where $x = (\pi M_z f)^{1/3}$ with $M_z = (1+z)M$ is the total redshifted mass with M representing the intrinsic total mass, ν representing the symmetric mass ratio $m_A m_B/(m_A + m_B)^2$ and f is the observed GW frequency. $P(x)$ is a Padé-resummed function given by

$$P(x) = \frac{1 + n_1 x + n_{3/2}x^{3/2} + n_2 x^2 + n_{5/2}x^{5/2} + n_3 x^3}{1 + d_1 x + d_{3/2}x^{3/2} + d_2 x^2}, \tag{14}$$

where the coefficients can be found in [60]. κ_{eff} is related to the tidal Love number k as

$$\kappa_{\text{eff}} = \frac{2}{13}\left[\left(1 + 12\frac{X_B}{X_A}\right)\left(\frac{X_A}{C_A}\right)^5 k^A + (A \leftrightarrow B)\right]. \tag{15}$$

Here, subscript A and B denotes the two component stars, $X_A \equiv m_A/M$ and the compactness is given by $C_A \equiv m_A/R_A$ with the stellar radius R_A. Since k depends on the intrinsic stellar mass instead of the redshifted one, the tidal effect can be used to extract the redshift information from a GW observation alone.

IV. FISHER ANALYSIS

In this paper, we carry out a parameter estimation based on a Fisher analysis [62], which is valid for sources with sufficiently large signal-to-noise ratios (SNRs). We perform two different Fisher calculations, one for the redshift estimate and another for the modified GW propagation parameter estimate. Below, we will explain each of these Fisher analyses in turn.

A. Redshift estimate

The first step is to estimate the measurability of the redshift by using template gravitational waveforms of BNSs, which we take as the (nonspinning) IMRPhenomD-NRTidalv2 waveform [60,61,63,64]. It consists of the IMRPhenomD waveform for point-particle binaries with an updated tidal effect added to the phase. The waveform $\tilde{h}$ in the frequency domain can be written as

$$\tilde{h}(f) = \tilde{A}(f)e^{-i\psi(f)}, \qquad (16)$$

where $\tilde{A}$ is the IMRPhenomD amplitude[2] while ψ is the phase given by[3]

$$\psi(f) = \psi_{\rm pp}(f) + \psi_{\rm T}(f). \qquad (17)$$

Here $\psi_{\rm pp}$ is the (nonspinning) point-particle term that is taken from the IMRPhenomD waveform while $\psi_{\rm T}$ is the tidal contribution given in Eq. (13) that is parametrized by the Love number k. In our analysis, we use the tidal deformability $\lambda \equiv (2/3)R^5 k$, which is a function of the NS mass m. It is convenient to Taylor expand $\lambda(m)$ about a fiducial mass m_0 as [30,59]

$$\begin{aligned} \lambda &= \lambda_0 + \lambda_1(m - m_0) + \mathcal{O}[(m - m_0)^2] \\ &= \tilde{\lambda}_0 + \tilde{\lambda}_1 m + \mathcal{O}[(m - m_0)^2], \end{aligned} \qquad (18)$$

where λ_i are the Taylor coefficients about m_0 while $\tilde{\lambda}_0 = \lambda_0 - \lambda_1 m_0$ and $\tilde{\lambda}_1 = \lambda_1$.

---

[2]The NRTidal waveform also has a tidal correction to the amplitude, though the tidal effect is mostly determined from the phase and thus we do not include such effects in the amplitude for simplicity.

[3]In this paper, we include the tidal phase only in the inspiral part of the IMRPhenomD phase, though we have checked that our results are unaffected even if we include the tidal phase also in the intermediate portion of the waveform.
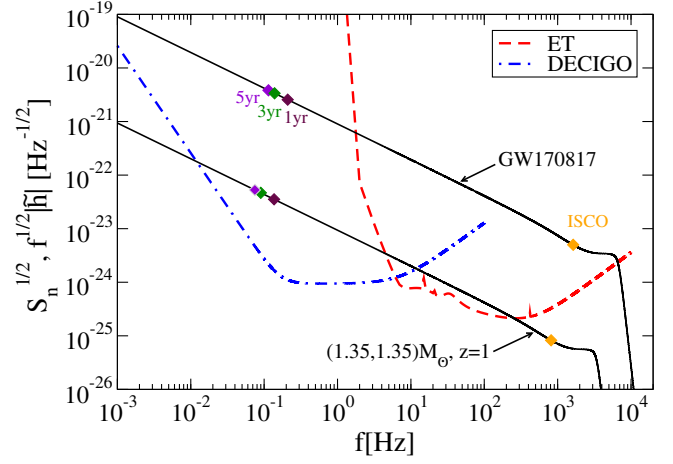

FIG. 2.   The noise spectral densities for ET [65] and DECIGO [66]. We also present the GW spectrum for GW170817 and a BNS with $(1.35, 1.35)$ $M_\odot$ at $z = 1$. For each GW spectrum, we show the frequency at ISCO and that at 1 yr, 3 yr, and 5 yr before coalescence.

One can compute the measurability of parameters θ^i from a Fisher matrix as follows. We first assume that the detector noise is stationary and Gaussian. Then, the probability distribution of θ^i becomes also Gaussian as

$$p(\theta^i) \propto \exp\left[-\frac{1}{2}\Gamma_{ij}(\theta^i - \hat{\theta}^i)(\theta^j - \hat{\theta}^j)\right], \qquad (19)$$

where $\hat{\theta}^i$ are the maximum likelihood parameters. Γ_{ij} is the Fisher matrix defined as

$$\Gamma_{ij} = 4\Re \int_{f_{\rm low}}^{f_{\rm high}} \frac{\partial_i \tilde{h} \partial_j \tilde{h}}{S_n(f)} df, \qquad (20)$$

where $\partial_i \equiv \partial/\partial\theta^i$ while S_n is the noise spectral density. $f_{\rm high}$ and $f_{\rm low}$ are the high and low frequency cutoffs to be discussed later.

$$\tilde{\Gamma}_{ij} = \sum_A \Gamma_{ij}^{(A)}, \qquad (21)$$

where A is the label of each detector. Finally, the 1σ root-mean-square error on θ_i is given by

$$\Delta\theta^i = \sqrt{(\tilde{\Gamma}^{-1})_{ii}}. \qquad (22)$$

In Fig. 2, we present S_n for ET and DECIGO, together with the GW spectrum for GW170817 and a BNS with $(1.35, 1.35)$ $M_\odot$ at $z = 1$. For ET, we choose the low and high frequency cutoffs in the Fisher matrix in Eq. (20) as

$$f_{\rm low}^{\rm (ET)} = 1 \text{ Hz}, \qquad f_{\rm high}^{\rm (ET)} = \min(f_{\rm ISCO}, f_{\rm cont}), \qquad (23)$$

where

$$f_{\rm ISCO} = \frac{1}{6^{3/2}\pi M_z},\qquad(24)$$

is the frequency at the innermost stable circular orbit (ISCO) while $f_{\rm cont}$ is the (redshifted) contact frequency of two NSs and is given by

$$f_{\rm cont} = \frac{1}{2^{3/2}\pi(1+z)}\sqrt{\frac{M}{R^3}},\qquad(25)$$

for an equal-mass BNS with R representing the stellar radius. For a NS with a soft (stiff) EOS, the radius is relatively small (large), and $f_{\rm ISCO} < f_{\rm cont}$ ($f_{\rm ISCO} > f_{\rm cont}$). On the other hand, for DECIGO, we choose the low and high cutoff frequencies as

$$f_{\rm low}^{\rm (DEC)} = 0.233\left(\frac{1\,M_\odot}{\mathcal{M}_z}\right)^{5/8}\left(\frac{1\,{\rm yr}}{T_{\rm obs}}\right)^{3/8}\,{\rm Hz},$$

$$f_{\rm high}^{\rm (DEC)} = 100\,{\rm Hz},\qquad(26)$$

where $\mathcal{M}_z = M_z\eta^{3/5}$ is the redshifted chirp mass, $T_{\rm obs}$ is the observation time and $f_{\rm low}^{\rm (DEC)}$ corresponds to the (redshifted) frequency at $T_{\rm obs}$ before coalescence.

Let us now explain parameters θ^i specific to our analysis. We use the sky-averaged waveform and the parameters are given by

$$\theta^i = (\ln\mathcal{M}_z, \eta, t_c, \phi_c, \ln A, \ln z).\qquad(27)$$

Here $\eta = m_1 m_2/M^2$ is the symmetric mass ratio with individual masses m_A, and t_c and ϕ_c are the coalescence time and phase respectively. The amplitude parameter A is given by $A = \mathcal{M}_z^{5/6}/(\sqrt{30}\pi^{2/3}d_L^{\rm gw})$, which corresponds to the leading, sky-averaged amplitude in the frequency domain without the frequency dependence [67]. We assume the tidal parameters $\tilde{\lambda}_0$ and $\tilde{\lambda}_1$ are known *a priori* from BNSs with $z < 0.1$ (we discuss how the imperfect knowledge of the EOS affects the measurability of the redshift in Appendix C). Regarding fiducial values for Fisher analyses, we choose $m_1 = m_2 = m_0 = 1.35\,M_\odot$, $t_c = 0$, $\phi_c = 0$, and vary z or $d_L^{\rm gw}$. Fiducial values for $\tilde{\lambda}_0$ and $\tilde{\lambda}_1$ are summarized in Table II in Appendix C for three EOSs as representatives of soft, intermediate and stiff classes: SLy [68], MPA1 [69] and MS1 [70].

B. Parameter estimation for modified GW propagation

We now move onto explaining the second Fisher analysis for estimating the measurability of cosmological parameters and the modified GW propagation parameter. We consider a spatially flat Universe and work on the following four parameters [25]:

TABLE II. Values of $\tilde{\lambda}_0[10^{36}\,{\rm g\,cm^2\,s^2}]$, $\tilde{\lambda}_1[(10^{36}\,{\rm g\,cm^2\,s^2}/M_\odot)]$ and their standard deviations for Gaussian priors for SLy and MS1. The priors are taken from the results of two cases under the detection of HLV in Sec. 5.4 in [59], the pessimistic case with 30 BNSs and the optimistic case with 384 BNSs.

| | SLy | | MS1 | |
	Pessimistic (30 BNSs)	Optimistic (384 BNSs)	Pessimistic (30 BNSs)	Optimistic (384 BNSs)
$\tilde{\lambda}_0$	4.46		12.41	
$\sigma_{\tilde{\lambda}_0}$	0.039	0.014	0.029	0.009
$\tilde{\lambda}_1$	−1.99		−3.35	
$\sigma_{\tilde{\lambda}_1}$	0.025	0.0125	0.019	0.009

$$p^i = (\ln H_0, \ln\Omega_M, w_0, \Xi_0).\qquad(28)$$

Here H_0 is the Hubble constant, Ω_M is the matter energy density parameter at present time, w_0 is the equation of state parameter for dark energy [71,72][4] while Ξ_0 is the modified GW propagation parameter in Eq. (3). The luminosity distance measured by EM observations depends only on the first three parameters in Eq. (28) as

$$d_L^{\rm em}(z) = (1+z)\int_0^z \frac{d\tilde{z}}{H(\tilde{z})},\qquad(29)$$

with the Hubble parameter given by

$$H(z) = H_0\sqrt{\Omega_M(1+z)^3 + (1-\Omega_M)(1+z)^{3(1+w_0)}}.\qquad(30)$$

We can construct a Fisher matrix to estimate the measurability of the parameters p^i by studying how $\ln d_L^{\rm gw}$ depends on each of these parameters and comparing it with a measurement error on $\ln d_L^{\rm gw}$. Combining information from multiple events, we can write down the Fisher matrix as [59]

$$F_{ij}^{\rm (A)} = \sum_a \frac{(\partial\ln d_L^{\rm gw}/\partial p_i)(\partial\ln d_L^{\rm gw}/\partial p_j)}{(\Delta\ln d_L^{\rm gw})_{\rm (A)}^2}\bigg|_a.\qquad(31)$$

Here a labels each BNS while $A = ({\rm gw, em})$ labels whether the redshift is measured from GWs through the tidal effects or from EM counterparts. $(\Delta\ln d_L^{\rm gw})_{\rm (A)}^2$ is the total error on $\ln d_L^{\rm gw}$ given by

$$(\Delta\ln d_L^{\rm gw})_{\rm (A)}^2 = (\Delta\ln d_L^{\rm gw})_{\rm gw}^2 + \epsilon_A\left(\frac{\partial\ln d_L^{\rm gw}}{\partial z}\Delta z\right)^2$$

$$+ (\Delta\ln d_L^{\rm gw})_{\rm lens}^2,\qquad(32)$$

---

[4]The equation of state for dark energy is given by $P_{\rm DE} = w_0\varepsilon_{\rm DE}$ where $P_{\rm DE}$ and $\varepsilon_{\rm DE}$ are the pressure and energy density of dark energy.

with $\epsilon_{gw} = 1$ and $\epsilon_{em} = 0$. The first term on the right-hand side is the measurement error on $\ln d_L^{gw}$ through GWs, the second term is due to the measurement error on the redshift, while the last term is due to the gravitational lensing given by [73]

$$(\Delta \ln d_L^{gw})_{lens} \simeq 0.05z. \quad (33)$$

The first two terms are computed from Γ_{ij} in the previous subsection, either with ET alone or with the multiband observations. For BNSs with redshift identified from EM counterparts, the measurement error on the redshift is typically negligible and we drop the second term in Eq. (32) (i.e., $\epsilon_{em} = 0$) for such cases.

In this paper, we follow [59] and assume that all BNSs are identical except for their redshifts. Under this assumption, one can turn the summation in F_{ij} into an integral as

$$F_{ij}^{(A)} = \int_{z_{min}}^{z_{max}} \frac{(\partial \ln d_L^{gw}/\partial p_i)(\partial \ln d_L^{gw}/\partial p_j)}{(\Delta \ln d_L^{gw})_{(A)}^2} \mathcal{R}(z)dz. \quad (34)$$

We choose the minimum and maximum redshifts (z_{min} and z_{max}) as $z_{min} = 0.1$ and $z_{max} = 2$. This is because we use BNS sources with $z < 0.1$ (with EM counterparts) to determine the NS EOS while the SNR becomes too small for detection when $z > 2$.[5] $\mathcal{R}(z)$ is the distribution of BNS mergers which is given by [75]

$$\mathcal{R}(z) = \frac{4\pi r^2(z)\dot{n}_0 s(z)}{H(z)(1+z)} T_{obs}, \quad (35)$$

in which $\dot{n}_0 = 10^{-6}$ Mpc^{-3} yr^{-1} [76] is the current BNS merger rate, $r(z)$ is the comoving distance, and

$$s(z) = \begin{cases} 1 + 2z & (z \leq 1) \\ \frac{3}{4}(5 - z) & (1 < z \leq 5) \end{cases}, \quad (36)$$

shows the redshift evolution of the merger rate. We show the BNS merger rate within each redshift bin and the accumulated merger rate up to a given redshift in Fig. 3.

Unlike the multiband GW observations of stellar-mass black hole binaries with ground-based detectors and LISA whose rate is much lower than that with ground-based detectors alone [31], the rate for joint detection of GWs from BNSs with ET + DECIGO is comparable or even higher than ET alone. This is because the signal-to-noise ratio (SNR) of BNS GW detection with DECIGO is higher than that of ET, as can be seen from Fig. 2. Thus, DECIGO

FIG. 3. The BNS merger rate per unit redshift ($\mathcal{R}(z)$) and the accumulated number of events up to a given redshift ($\int_0^{\tilde{z}} \mathcal{R}(z)dz$) as a function of z.

can detect GW signals from BNSs whose signals can also be detected with ET. Moreover, since DECIGO will be able to give a precursor alert to ET, the detection SNR threshold may be lowered (as we explain in footnote 5), which will increase the rate compared to the case with ET alone.

Given that various cosmological observations, including cosmic microwave background (CMB), baryon acoustic oscillation (BAO) and supernovae, measured cosmological parameters with some errors, one can impose prior on such parameters for our Fisher analysis. For simplicity, we impose Gaussian priors with standard deviation $\sigma_{p_i}^0$ for each parameter. The Fisher matrix for BNSs with redshift identification due to EM counterparts is given by

$$\tilde{F}_{ij}^{(em)} = \alpha F_{ij}^{(em)} + \frac{\delta_{ij}}{(\sigma_{p^i}^0)^2}. \quad (37)$$

Here α is the fraction of total BNSs with which the redshifts are identified through their EM counterparts [41]. One can further add BNSs whose redshift is identified through the tidal measurement of GWs as

$$\tilde{F}_{ij}^{(gw+em)} = (1 - \alpha)F_{ij}^{(gw)} + \alpha F_{ij}^{(em)} + \frac{\delta_{ij}}{(\sigma_{p^i}^0)^2}. \quad (38)$$

The 1-σ root-mean-square error on p^i can be estimated as

$$\Delta p^i = \sqrt{(\tilde{F}^{-1})_{ii}}. \quad (39)$$

We end this section by describing the fiducial values and priors for p^i. For the former, we use $H_0 = 67.64$ km s^{-1} Mpc^{-1}, $\Omega_M = 0.3087$, $w_0 = -1$, $\Xi_0 = 1$. This corresponds to the ΛCDM model in GR with the first two parameter values being the best-fit values from CMB, BAO and supernovae observations [25]. For the prior, we use [25]

---

[5]The SNR for a sky-averaged BNS at $z = 2$ with ET is 4.5 which may be smaller than the detection threshold SNR, though the latter may be reduced if we have additional information from DECIGO for multiband observations (see, e.g., [74] for a related work).
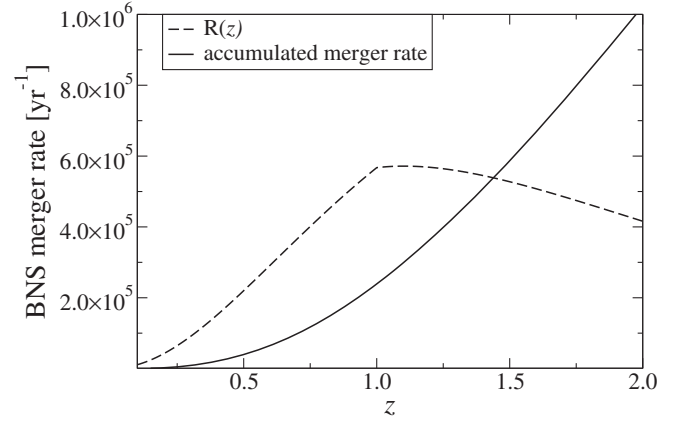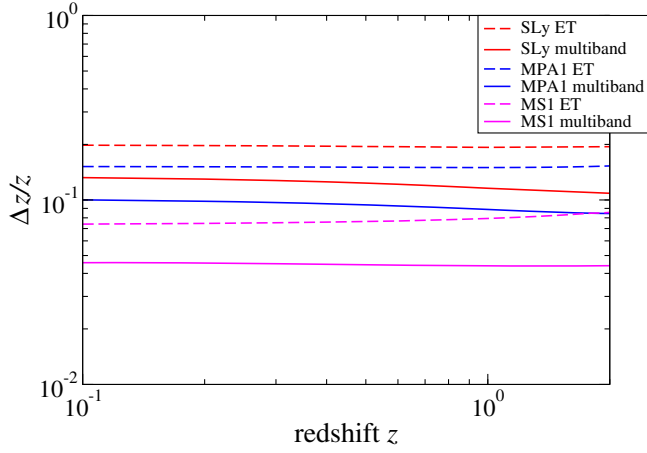
FIG. 4. The fractional uncertainty of the redshift as a function of the source redshift with ET and multiband GW observations (with a 3-yr observation for the latter). We present the results for SLy (soft) [68], MPA1 (intermediate) [69] and MS1 (stiff) [70] EOSs. Notice that the uncertainty is insensitive to z and is larger for softer EOSs.

$$(\sigma^0_{\Xi_0}, \sigma^0_{\omega_0}, \sigma^0_{\ln H_0}, \sigma^0_{\ln \Omega_M}) = (\infty, 0.0535, 0.018, 0.039), \quad (40)$$

which is obtained from the same datasets as those for the above fiducial values.

V. RESULTS

We now present our main results. We first show the measurability of redshift with GW observations. We next use this to compute the measurability of the modified GW propagation parameter Ξ_0 and cosmological parameters. We finally map the projected bounds on Ξ_0 to those on example theories within the Horndeski class and example phenomenological models.

A. Redshift inference

We begin by showing the measurement accuracy of z with GW observations using ET and multiband (ET + DECIGO) detections in Fig. 4 for the three representative EOSs. Observe that the redshift can be measured to $\mathcal{O}(10\%)$ and is insensitive to the BNS redshift. Notice also that the measurability of z increases as the EOS becomes stiffer. This is because the NS radius becomes larger and the tidal effect in turn becomes stronger. We further see that the multiband detection improves the measurability of z from the case with ET alone by $\sim 50\%$. The result for ET in Fig. 4 is consistent with that in [30]. The difference originates from using, e.g., different point-particle waveforms (IMRPhenomD v.s. Taylor F2) and tidal effects (5 and 6PN v.s. NRTidal fit).

Before showing bounds on Ξ_0, let us first present in Fig. 5 different errors on the luminosity distance [Eq. (32)] in the second Fisher matrix F_{ij}. We chose SLy EOS and the multiband observation. Notice that the error propagated
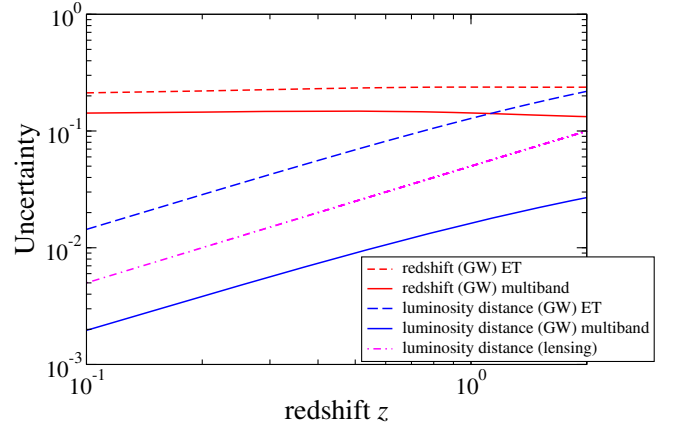

FIG. 5. Various sources of the luminosity distance measurement uncertainties in Eq. (32) as a function of the BNS redshift. We use the SLy EOS and assume multiband observations (with a 3-yr observation time). Notice that the redshift uncertainty dominates the error budget throughout.

from the redshift measurement in Fig. 4 dominates the other two errors (direct measurement of d_L^{gw} from GWs and the lensing) for both ET alone and multiband observations. On the other hand, when there is an EM counterpart, the error from redshift is negligible and it is the lensing (direct luminosity distance measurement) error that gives the dominant contribution for multiband (ET alone) observations.

B. Constraints on GW propagation parameter Ξ_0

Having the redshift measurability at hand, we next present the measurability of the modified GW propagation parameter Ξ_0. Figure 1 in Sec. I presents such a measurement error on Ξ_0 for $n = 2.5$ against the fraction α of the redshift identification of BNSs through EM counterparts for ET and multiband observations. We show the results using BNSs with EM counterparts only (whose redshifts are identified), and combining BNSs with and without the counterparts. We chose the SLy EOS and an observation time of 3 yrs for DECIGO in the multiband observations (see Appendix B for how the results change with a different choice of EOSs and observation time). Notice first that the addition of BNS events without EM counterparts improves the measurability of Ξ_0 from the case with EM counterparts alone by a factor of a few. Notice also that for the combined case, BNSs with EM counterparts have a noticeable contribution when $\alpha \gtrsim 0.1$ for ET alone and $\alpha \gtrsim 0.01$ for multiband observations (where the red curves drop). Furthermore, when $\alpha \sim 1$ (i.e., most of BNSs have EM counterparts), multiband observations significantly improve the bound on Ξ_0 from the case with ET alone. This is because when $\alpha \sim 1$, the error budget in the luminosity distance measurement is different between ET and multiband cases as already explained in Sec. V A and in Fig. 5.
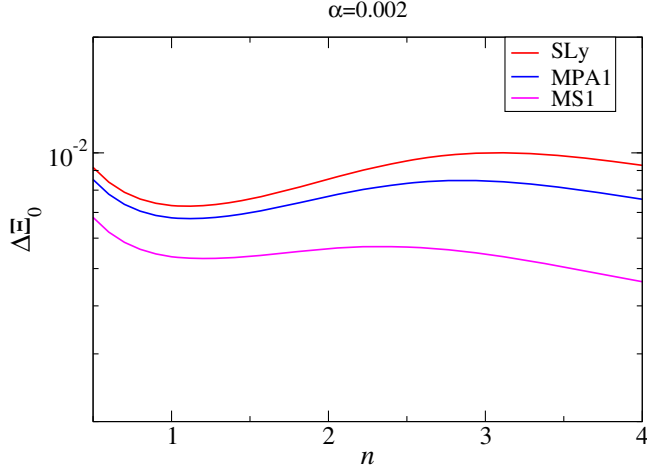
FIG. 6.   Measurability of Ξ_0 against the index n in the modified GW luminosity distance in Eq. (3) for three representative EOSs. We consider a multiband observation with combined BNS events with and without EM counterparts. We fix the fraction of BNSs with EM counterparts as $\alpha = 2 \times 10^{-3}$. The observational time is 3 years. Observe that the measurability is not very sensitive to the choice of n.

Next, Fig. 6 presents the measurability of Ξ_0 against the index n in the luminosity distance ratio expression [Eq. (3)] for a multiband observation with combined BNS events (both with and without redshift identification through EM counterparts) for $\alpha = 2 \times 10^{-3}$.[6] We show the results for the three representative EOSs. Notice first that the measurement error of Ξ_0 is mostly insensitive to n and varies only by $\sim 20\%$. Notice also that the error decreases for stiffer EOSs (MS1), which is consistent with the measurement error of z in Fig. 4.

C. Mapping to Horndeski theories

Finally, we consider mapping the bounds on the modified GW propagation parameter Ξ_0 to those on scalar-tensor theories and phenomenological models. The top panel of Fig. 7 shows bounds on the HS $f(R)$ gravity $|f_{R0}|$ and Brans-Dicke theory $|\delta\phi_0|$ as a function of α for various choices of the positive integer $\bar{n}$. Observe that the addition of BNSs with redshift identification through tidal measurements and the use of multiband observations improve the bounds on these theories from the case with ET observations of BNSs with EM counterparts by a factor of 2–10. Observe also that the bounds are insensitive to a variation in $\bar{n}$, especially for the multiband case.

---

[6]The fraction $\alpha = 2 \times 10^{-3}$ is derived for short gamma-ray bursts assuming that 2% of them points to us and only 10% of them can have measurable redshift due to noisy spectrum, dimming at high redshift, etc. [41]. This fraction can be larger for other sources, such as kilonova, or if we take into account off-axis emission.
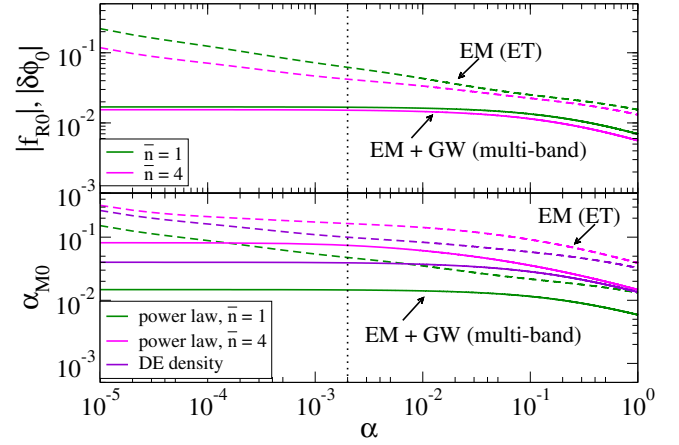

FIG. 7.   Top: projected bounds on parameters in the HS $f(R)$ gravity ($|f_{R0}|$) and Brans-Dicke theory ($|\delta\phi_0|$) as a function of the fraction α for redshift identification through EM counterparts. We present the bounds for the following two cases: (i) GW observations of BNSs with ET where the sources' redshifts are identified through EM counterparts only (dashed), and (ii) multiband GW observations of BNSs whose redshifts are identified through either EM counterparts or GW tidal effects (solid). For each case, we show the bounds for two choices of the positive index $\bar{n}$. We assume 3-year observations and the SLy EOS. The dashed vertical line at $\alpha = 2 \times 10^{-3}$ [41] corresponds to an example value for the fraction of BNSs with redshift identification. Bottom: a similar bound on the phenomenological α_M models in Eqs. (11) and (12).

Similarly, the bottom panel of Fig. 7 presents bounds on α_{M0} in the two phenomenological models mentioned in Sec. II B 2. Notice that the amount of improvement on the bounds with the addition of BNSs without EM counterparts and multiband observations is similar to those on scalar-tensor theories in Fig. 7. Notice also that the variation in $\bar{n}$ is larger for this case than that for scalar-tensor theories in the top panel.

VI. CONCLUSIONS AND DISCUSSIONS

In this paper, we considered using GWs from BNS mergers both with and *without* EM counterparts to probe a modified GW propagation effect in the amplitude due to a modified friction in the tensor perturbation evolution. For the events without EM counterparts, we use the tidal information to break the degeneracy between the redshift and the mass [30]. We found that by including BNSs without EM counterparts and using multiband GW observations between ET and DECIGO, one can improve the measurability on the modified GW propagation parameter Ξ_0 by a factor of a few compared to the case with ET observations of BNSs with EM counterparts that has been studied previously. We further mapped these projected bounds on Ξ_0 to those on specific non-GR theories and phenomenological models. For example, we found that a parameter in an $f(R)$ gravity can be constrained to

$|f_{R0}| \lesssim 10^{-2}$. These findings show the impact of using the tidal information and multiband observations to probe a modified GW propagation (or modified friction) effect entering in the waveform amplitude.

We end by presenting possible directions for future avenues. One could improve the analysis here by carrying out a Bayesian parameter estimation study (instead of a Fisher analysis) and drawing BNSs from a population model to allow for different parameters (like masses). One should also relax the sky-averaged assumption and account for sky location and orientation of a BNS. This could be important given that there was a strong correlation between the luminosity distance and the inclination angle for GW170817 [77]. However, in Appendix D, we carried out an additional analysis by relaxing the sky-averaged assumption for DECIGO and showed that in most cases, the measurement error for the luminosity distance is still smaller than that from the redshift measurement. This suggests that the result presented here with the sky-averaged analysis should not change much for multiband observations even if one accounts for the correlation. It would be also important to take into account systematic uncertainties due to imperfect knowledge of the EOS and certain universal relations may help to break the degeneracy among various tidal parameters [78–82]. Lastly, one could also attempt to combine the tidal method presented here with other approaches that do not require EM counterparts, such as correlating dark sirens with galaxy catalogs [28,83,84] or using the known NS mass distribution [85,86].

APPENDIX A: ADDITIONAL SCALAR-TENSOR THEORY AND PHENOMENOLOGICAL MODEL

In this Appendix, we present the mapping between the modified GW propagation parameters (Ξ_0, n) to additional scalar-tensor theories and phenomenological models, and present future projected bounds on these theories/models through tidal measurement of BNS mergers. The mapping is summarized in Table I.

(i) *Designer $f(R)$ gravity* [54]: Other than the HS model, an interesting $f(R)$ gravity model includes the designer model that exactly reproduces the standard cosmological expansion history. The model is characterized by the Compton wavelength parameter
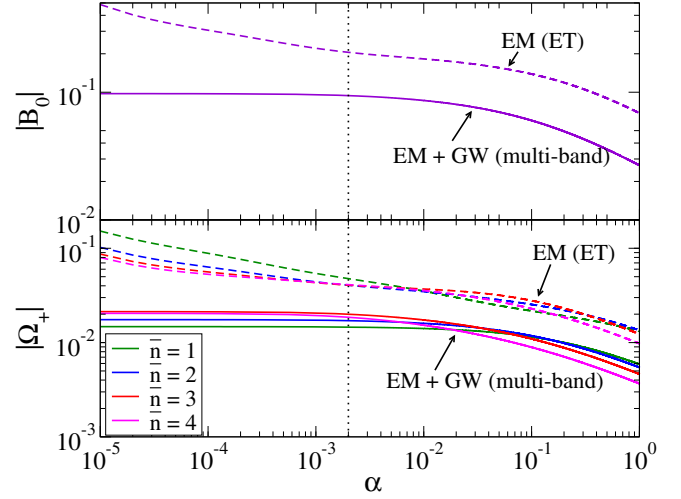

FIG. 8. Similar to Fig. 7 but for the bounds on the Compton wavelength parameter $|B_0|$ in the designer $f(R)$ gravity (top) and $|\Omega_+|$ in the power law $M_{\rm eff}$ formalism (bottom).

$$B_0 \equiv \left.\frac{Hf_R'}{H'(1+f_R)}\right|_0 \approx -2.1\Omega_M^{-0.76}f_{R0}. \quad (A1)$$

The top panel of Fig. 8 presents the bound on $|B_0|$ with GWs from BNSs using a three-year observation of a multiband network as a function of α. We used $n = 2.34$, which is close to $n = 2.5$ in Fig. 1 and thus follows the same trend. Observe that the bounds on B_0 increases by a factor of 2–5 if we add BNS events without EM counterparts.

(ii) *power law $M_{\rm eff}$*: On top of the phenomenological models for α_M, we consider a phenomenological model on the effective Planck mass $M_{\rm eff}$. As an example, we consider a simple power law model for $M_{\rm eff}^2$ given by [58]

$$M_{\rm eff}^2 = \frac{1}{8\pi}(1 + \Omega_+ a^{\bar{n}}), \quad (A2)$$

where Ω_+ and $\bar{n}$ are constant parameters. α_M in this model is given by

$$\alpha_M = \frac{\bar{n}\Omega_+ a^{\bar{n}-1}}{1 + \Omega_+ a^{\bar{n}}}. \quad (A3)$$

Using the mapping in Table I, we present in the bottom panel of Fig. 8 the projected bounds on $|\Omega_+|$ for BNSs with and without EM counterparts for various $\bar{n}$. Observe that the addition of BNSs without EM counterparts improve the bound by an order of magnitude for small α and $\bar{n}$. On the other hand, the improvement is by a factor of a few irrespective of $\bar{n}$ when $\alpha \sim 1$.
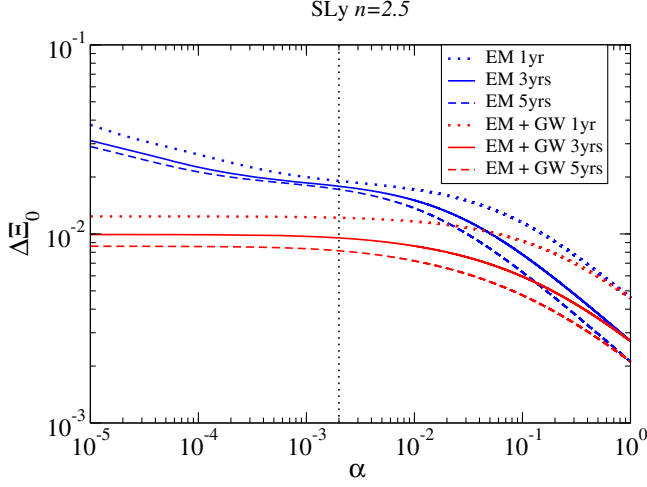
FIG. 9. Measurement errors on the modified GW propagation parameter Ξ_0 as a function of α for three different observation periods. We consider BNSs with redshift identified from EM counterparts only (blue), as well as those with redshift identification by EM and GW observations (red). We fix $n = 2.5$, choose the SLy EOS and consider multiband observations.

APPENDIX B: OBSERVATION TIME AND EOS DEPENDENCE ON $\Delta\Xi_0$

In this Appendix, we carry out some additional investigations on the measurability of Ξ_0 with multiband GW observations. Figure 9 presents how $\Delta\Xi_0$ depends on the observation period. Notice that the observation time has the most significant effect when $\alpha \sim 1$. For this case, the error on the luminosity distance measurement is dominated by the lensing that is independent of the observation time. Moreover, the prior on the second Fisher matrix $\tilde{F}_{ij}$ in Eq. (37) is less important and the measurability scales with $T_{\text{obs}}^{-1/2}$ since the number of BNS events increases linearly with T_{obs} [see Eq. (35)]. On the other hand, for smaller α, the prior on $\tilde{F}_{ij}$ becomes more important and the above scaling breaks down. Notice also that the observation time has a larger effect on the case with all BNSs (with and without EM counterparts) than BNSs with EM counterparts only. This is because for the former, the error on the luminosity distance measurement is dominated by the redshift uncertainty, and a longer observation time helps more to break the degeneracy between the redshift and other parameters.

Figure 10 presents $\Delta\Xi_0$ with multiband observations for the three representative EOSs. For the case with BNSs with EM counterparts alone, EOS only affects the first Fisher matrix $\tilde{\Gamma}_{ij}$ through the maximum frequency cutoff. Since the effect is small, we only consider the SLy EOS for this case. Notice that the measurability of Ξ_0 improves as we make the EOS stiffer. This is as expected from the measurability of the redshift from Fig. 4.
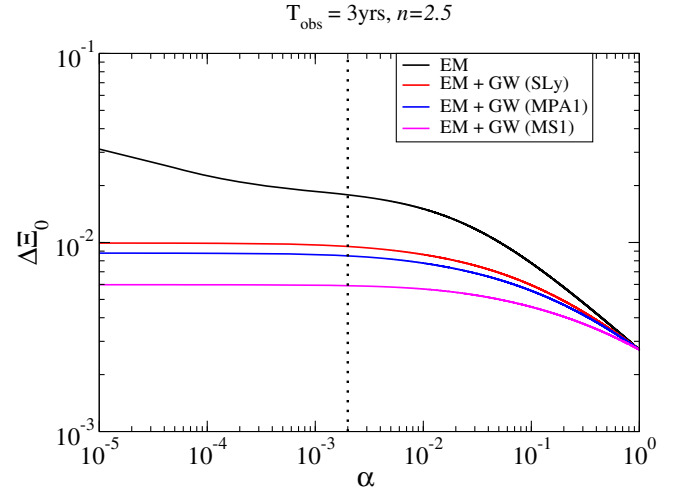

FIG. 10. Similar to Fig. 9 but showing how $\Delta\Xi_0$ varies with EOSs. We fix $T_{\text{obs}} = 3$ yrs and $n = 2.5$.

APPENDIX C: INCLUSION OF $\tilde{\lambda}_0$ AND $\tilde{\lambda}_1$

In this Appendix, we study how the imperfect knowledge of the EOS may affect the measurability of the redshift. For this, we include $\tilde{\lambda}_0$ and $\tilde{\lambda}_1$ into a search parameter set θ^i in Eq. (27) for the first Fisher analysis:

$$\theta^i = (\ln \mathcal{M}_z, \eta, t_c, \phi_c, \ln A, \ln \tilde{\lambda}_0, \ln \tilde{\lambda}_1, \ln z). \quad \text{(C1)}$$

For simplicity, we follow [62,87] and assume a Gaussian prior with standard deviations $\sigma_{\tilde{\lambda}_0}$ and $\sigma_{\tilde{\lambda}_1}$. The effective Fisher matrix now becomes

$$\tilde{\Gamma}_{ij} = \sum_A \Gamma_{ij}^{(A)} + \frac{\delta_{ij}}{(\sigma_{\theta^i})^2}. \quad \text{(C2)}$$

To give an example, we consider a prior for $\tilde{\lambda}_0$ and $\tilde{\lambda}_1$ that corresponds to measuring them through a network of LIGO Hanford/Livingston and Virgo (HLV) shown in Table II that is taken from [59]. Following this reference, we assume that all BNSs with $z < 0.1$ detected through such a network has EM counterparts and can be used to measure $\tilde{\lambda}_0$ and $\tilde{\lambda}_1$. This is somewhat optimistic, though the authors in [59] found that the measurability of these tidal parameters do not change much even if one only uses BNSs with $z < 0.05$.

Figure 11 presents the measurability of the redshift for multiband GW observations where $\tilde{\lambda}_0$ and $\tilde{\lambda}_1$ are included in the search parameter for Fisher analyses for the SLy and MS1 EOSs. We consider a pessimistic (optimistic) case with 30 (384) detected BNSs with $z < 0.1$ for a 3-yr observation. For reference, we show the result without $\tilde{\lambda}_0$ and $\tilde{\lambda}_1$ in the search parameter set from Fig. 4. Notice that the uncertainty in the EOS affects the measurability of the redshift only for BNSs with low z. Moreover, such an uncertainty on the EOS will be reduced if one uses ET
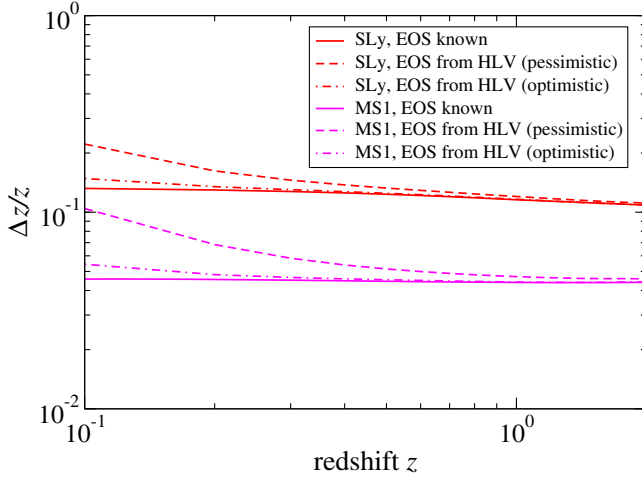
FIG. 11. The measurability of the redshift with multiband GW observations for the case where (i) the EOS is known *a priori* and (ii) $\tilde{\lambda}_0$ and $\tilde{\lambda}_1$ are obtained from a network of HLV observations [59]. For the latter, we consider both pessimistic (30 BNSs) and optimistic cases (384 BNSs) for 3-yr observations. We show the results for SLy (soft) and MS1 (stiff) EOS.
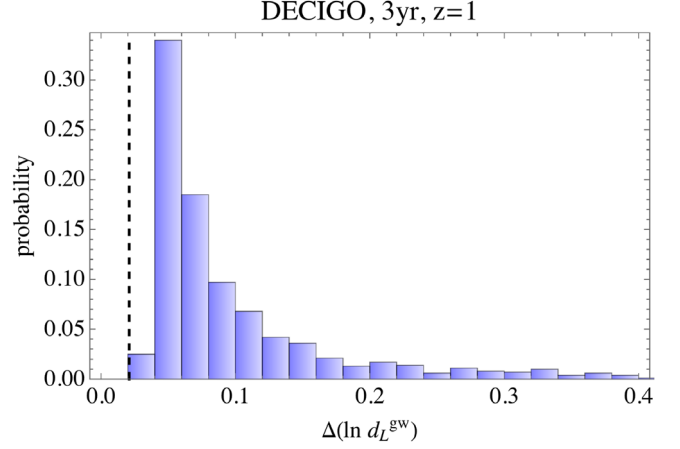

FIG. 12. Histogram for the probability of the luminosity distance measurability with DECIGO for at $z = 1$ whose sky location and orientation are randomly distributed. The black dashed vertical line shows the measurability with the sky-averaged case. Notice that most of binaries have the fractional error of less than 10% even if we account for the degeneracy between d_L^{gw} and binary orientations.

instead of LHV. We thus expect the effect of imperfect knowledge of the EOS to be small and neglect them in the main text.

APPENDIX D: DEGENERACY BETWEEN LUMINOSITY DISTANCE AND BINARY ORIENTATION

In this Appendix, we estimate the amount of degeneracy between the luminosity distance and binary orientation for multiband observations. Since the measurability of the luminosity distance for the multiband observation is mostly determined by observations with DECIGO (due to its high SNR and a large effective baseline of 1 AU), we focus on the latter for simplicity. The binary inclination varies over time due to the motion of DECIGO, and thus it is useful to work in a barycentric frame (centered at the Sun) [67,88–90]. In such a frame, we can describe the sky location of a BNS by (θ_s, ϕ_s) and the direction of its orbital angular momentum as (θ_L, ϕ_L). Following [90], we perform a new Fisher analysis with search parameters given by[7]

---

[7]In this Appendix, we do not include z since we focus on DECIGO which is insensitive to the effect close to merger. This does not affect the luminosity distance measurement since the amplitude parameters are mostly uncorrelated with the phase parameters.

$$\theta^i = (\ln \mathcal{M}_z, \eta, t_c, \phi_c, \ln A, \theta_s, \phi_s, \theta_L, \phi_L), \quad \text{(D1)}$$

and we take into account the motion of the detectors. We use a restricted post-Newtonian waveform where we only consider the leading Newtonian contribution for the amplitude while we include up to 2PN order in the phase. We carry out a Monte Carlo simulation in which we consider 10^3 BNSs at $z = 1$ with the angle parameters randomly drawn from a uniformly distribution in $\cos\theta_s$, ϕ_s, $\cos\theta_L$ and ϕ_L [67,89,90].

Figure 12 presents the distribution of the luminosity distance measurability for a 3-yr observation with DECIGO for BNSs at $z = 1$. For comparison, we also show the measurability when we use a sky-averaged waveform as done in the main part of this paper, which roughly agrees with the blue solid curve in Fig. 5 at $z = 1$ (suggesting that the error is indeed determined from the DECIGO measurement for multiband observations). Notice that although the sky-averaged analysis underestimates the error, the measurement error is below 10% for most of BNSs and thus does not exceed the error on the luminosity distance from the redshift measurement. This shows that the bound on Ξ_0 for multiband observations found in this paper through the sky-averaged analysis will not be affected much even if we include the effect of binary sky location and orientation.

[1] B. P. Abbott *et al.* (LIGO Scientific Collaboration and Virgo Collaboration), Phys. Rev. Lett. **116,** 061102 (2016).

[2] R. Abbott *et al.* (LIGO Scientific and Virgo Collaborations), arXiv:2010.14527 [Phys. Rev. X (to be published)].

[3] B. P. Abbott *et al.* (LIGO Scientific Collaboration and Virgo Collaboration), Phys. Rev. Lett. **119,** 161101 (2017).

[4] B. P. Abbott *et al.* (LIGO Scientific, Virgo, Fermi-GBM and INTEGRAL Collaborations), Astrophys. J. Lett. **848,** L13 (2017).

[5] B. P. Abbott, R. Abbott, T. D. Abbott, S. Abraham, F. Acernese, K. Ackley, C. Adams, R. X. Adhikari, V. B. Adya, C. Affeldt *et al.*, Astrophys. J. **892,** L3 (2020).

[6] LIGO Scientific, Virgo, 1M2H, Dark Energy Camera GW-EM, DES, DLT40, Las Cumbres Observatory, VINROUGE and MASTER Collaborations, Nature (London) **551,** 85 (2017).

[7] M. Fishbach *et al.*, Astrophys. J. **871,** L13 (2019).

[8] H.-Y. Chen, M. Fishbach, and D. E. Holz, Nature (London) **562,** 545 (2018).

[9] A. Joyce, B. Jain, J. Khoury, and M. Trodden, Phys. Rep. **568,** 198 (2015).

[10] T. Clifton, P. G. Ferreira, A. Padilla, and C. Skordis, Phys. Rep. **513,** 1189 (2012).

[11] H. Nastase, arXiv:1112.3502.

[12] B. Jain and J. Khoury, Ann. Phys. (Amsterdam) **325,** 1479 (2010).

[13] V. Salvatelli, F. Piazza, and C. Marinoni, J. Cosmol. Astropart. Phys. 09 (2016) 027.

[14] M. Milgrom, Astrophys. J. **270,** 365 (1983).

[15] B. Famaey and S. S. McGaugh, Living Rev. Relativity **15,** 10 (2012).

[16] E. Belgacem, Y. Dirian, S. Foffa, E. J. Howell, M. Maggiore, and T. Regimbau, J. Cosmol. Astropart. Phys. 015 (2019) 1907.

[17] C. M. Will, Living Rev. Relativity **17,** 4 (2014).

[18] I. H. Stairs, Living Rev. Relativity **6,** 5 (2003).

[19] N. Wex, arXiv:1402.5594.

[20] B. P. Abbott *et al.* (LIGO Scientific and Virgo Collaborations), Phys. Rev. Lett. **116,** 221101 (2016); **121,** 129902(E) (2018).

[21] N. Yunes, K. Yagi, and F. Pretorius, Phys. Rev. D **94,** 084002 (2016).

[22] E. Berti, K. Yagi, and N. Yunes, Gen. Relativ. Gravit. **50,** 46 (2018).

[23] R. Abbott *et al.* (T. L. S. Collaboration and the Virgo Collaboration), arXiv:2010.14529.

[24] Z. Carson and K. Yagi, arXiv:2011.02938.

[25] E. Belgacem, Y. Dirian, S. Foffa, and M. Maggiore, Phys. Rev. D **98,** 023510 (2018).

[26] M. Lagos, M. Fishbach, P. Landry, and D. E. Holz, Phys. Rev. D **99,** 083504 (2019).

[27] R. DAgostino and R. C. Nunes, Phys. Rev. D **100,** 044041 (2019).

[28] A. Finke, S. Foffa, F. Iacovelli, M. Maggiore, and M. Mancarella, arXiv:2101.12660.

[29] S. Mukherjee, B. D. Wandelt, and J. Silk, Mon. Not. R. Astron. Soc. **502,** 1136 (2021).

[30] C. Messenger and J. Read, Phys. Rev. Lett. **108,** 091101 (2012).

[31] A. Sesana, Phys. Rev. Lett. **116,** 231102 (2016).

[32] E. Barausse, N. Yunes, and K. Chamberlain, Phys. Rev. Lett. **116,** 241104 (2016).

[33] S. Isoyama, H. Nakano, and T. Nakamura, Prog. Theor. Exp. Phys. **2018,** 073E01 (2018).

[34] Z. Carson and K. Yagi, Classical Quant. Grav. **37,** 02LT01 (2020).

[35] C. Cutler *et al.*, arXiv:1903.04069.

[36] Z. Carson and K. Yagi, Phys. Rev. D **101,** 044047 (2020).

[37] A. Gupta, S. Datta, S. Kastha, S. Borhanian, K. G. Arun, and B. S. Sathyaprakash, Phys. Rev. Lett. **125,** 201101 (2020).

[38] S. Datta, A. Gupta, S. Kastha, K. G. Arun, and B. S. Sathyaprakash, Phys. Rev. D **103,** 024036 (2021).

[39] S. Kawamura *et al.*, J. Phys. Conf. Ser. **122,** 012006 (2008).

[40] S. Kawamura *et al.*, arXiv:2006.13545.

[41] A. Nishizawa, K. Yagi, A. Taruya, and T. Tanaka, Phys. Rev. D **85,** 044047 (2012).

[42] B. F. Schutz, Nature (London) **323,** 310 (1986).

[43] M. Fishbach *et al.* (LIGO Scientific and Virgo Collaborations), Astrophys. J. Lett. **871,** L13 (2019).

[44] I. D. Saltas, I. Sawicki, L. Amendola, and M. Kunz, Phys. Rev. Lett. **113,** 191101 (2014).

[45] A. Nishizawa, Phys. Rev. D **97,** 104037 (2018).

[46] S. Mastrogiovanni, D. A. Steer, and M. Barsuglia, Phys. Rev. D **102,** 044009 (2020).

[47] G. W. Horndeski, Int. J. Theor. Phys. **10,** 363 (1974).

[48] T. Kobayashi, Rep. Prog. Phys. **82,** 086901 (2019).

[49] B. P. Abbott *et al.* (LIGO Scientific and Virgo Collaborations), Phys. Rev. Lett. **119,** 161101 (2017).

[50] D. Bettoni, J. M. Ezquiaga, K. Hinterbichler, and M. Zumalacrregui, Phys. Rev. D **95,** 084029 (2017).

[51] R. Kimura and K. Yamamoto, J. Cosmol. Astropart. Phys. 07 (2012) 050.

[52] R. McManus, L. Lombriser, and J. Pearrubia, J. Cosmol. Astropart. Phys. 11 (2016) 006.

[53] W. Hu and I. Sawicki, Phys. Rev. D **76,** 064004 (2007).

[54] Y.-S. Song, W. Hu, and I. Sawicki, Phys. Rev. D **75,** 044004 (2007).

[55] C. Brans and R. H. Dicke, Phys. Rev. **124,** 925 (1961).

[56] E. Bellini and I. Sawicki, J. Cosmol. Astropart. Phys. 07 (2014) 050.

[57] F. Simpson, C. Heymans, D. Parkinson, C. Blake, M. Kilbinger, J. Benjamin, T. Erben, H. Hildebrandt, H. Hoekstra, T. D. Kitching *et al.*, Mon. Not. R. Astron. Soc. **429,** 2249 (2013).

[58] L. Lombriser and A. Taylor, J. Cosmol. Astropart. Phys. 03 (2016) 031.

[59] B. Wang, Z. Zhu, A. Li, and W. Zhao, Astrophys. J. Suppl. Ser. **250,** 6 (2020).

[60] T. Dietrich, A. Samajdar, S. Khan, N. K. Johnson-McDaniel, R. Dudi, and W. Tichy, Phys. Rev. D **100,** 044003 (2019).

[61] T. Dietrich, S. Bernuzzi, and W. Tichy, Phys. Rev. D **96,** 121501 (2017).

[62] C. Cutler and E. E. Flanagan, Phys. Rev. D **49,** 2658 (1994).

[63] S. Husa, S. Khan, M. Hannam, M. Pürrer, F. Ohme, X. J. Forteza, and A. Bohé, Phys. Rev. D **93,** 044006 (2016).

[64] S. Khan, S. Husa, M. Hannam, F. Ohme, M. Pürrer, X. J. Forteza, and A. Bohé, Phys. Rev. D **93,** 044007 (2016).

[65] S. Hild *et al.*, Classical Quant. Grav. **28**, 094013 (2011).

[66] K. Yagi and N. Seto, Phys. Rev. D **83**, 044011 (2011).

[67] E. Berti, A. Buonanno, and C. M. Will, Phys. Rev. D **71**, 084025 (2005).

[68] F. Douchin and P. Haensel, Astron. Astrophys. **380**, 151 (2001).

[69] H. Mther, M. Prakash, and T. Ainsworth, Phys. Lett. B **199**, 469 (1987).

[70] H. Mller and B. D. Serot, Nucl. Phys. **A606**, 508 (1996).

[71] M. Chevallier and D. Polarski, Int. J. Mod. Phys. D **10**, 213 (2001).

[72] E. V. Linder, Phys. Rev. Lett. **90**, 091301 (2003).

[73] B. S. Sathyaprakash, B. F. Schutz, and C. Van Den Broeck, Classical Quant. Grav. **27**, 215006 (2010).

[74] K. W. Wong, E. D. Kovetz, C. Cutler, and E. Berti, Phys. Rev. Lett. **121**, 251102 (2018).

[75] C. Cutler and J. Harms, Phys. Rev. D **73**, 042001 (2006).

[76] B. P. Abbott *et al.* (LIGO Scientific Collaboration and Virgo Collaboration), Phys. Rev. X **9**, 031040 (2019).

[77] B. P. Abbott *et al.* (LIGO Scientific and Virgo Collaborations), Phys. Rev. X **9**, 011001 (2019).

[78] K. Yagi and N. Yunes, Classical Quant. Grav. **33**, 13LT01 (2016).

[79] K. Yagi and N. Yunes, Classical Quant. Grav. **34**, 015006 (2017).

[80] K. Yagi and N. Yunes, Phys. Rep. **681**, 1 (2017).

[81] K. Chatziioannou, C.-J. Haster, and A. Zimmerman, Phys. Rev. D **97**, 104036 (2018).

[82] B. P. Abbott *et al.* (LIGO Scientific and Virgo Collaborations), Phys. Rev. Lett. **121**, 161101 (2018).

[83] W. Del Pozzo, Phys. Rev. D **D86**, 043011 (2012).

[84] B. P. Abbott *et al.* (LIGO Scientific and Virgo Collaborations), arXiv:1908.06060.

[85] S. R. Taylor, J. R. Gair, and I. Mandel, Phys. Rev. D **85**, 023535 (2012).

[86] S. R. Taylor and J. R. Gair, Phys. Rev. D **D86**, 023502 (2012).

[87] E. Poisson and C. M. Will, Phys. Rev. D **52**, 848 (1995).

[88] C. Cutler, Phys. Rev. D **57**, 7089 (1998).

[89] K. Yagi and T. Tanaka, Phys. Rev. D **81**, 064008 (2010); **81**, 109902(E) (2010).

[90] K. Yagi and T. Tanaka, Prog. Theor. Phys. **123**, 1069 (2010).